Bone Reports 7 (2017) 137–144

Contents lists available at ScienceDirect

Bone Reports

journal homepage: www.elsevier.com/locate/bonr

Second-harmonic generation imaging of collagen in ancient bone

B. Thomas[a,*], D. McIntosh[a], T. Fildes[a,b], L. Smith[b], F. Hargrave[b], M. Islam[c], T. Thompson[c], R. Layfield[d], D. Scott[d], B. Shaw[d], C.L. Burrell[e], S. Gonzalez[e], S. Taylor[a]

[a] Mass Spectrometry Research Group, University of Liverpool, Brownlow Hill, Liverpool L69 3GJ, UK
[b] Norton Priory Museum, Runcorn WA7 1SX, UK
[c] School of Science and Engineering, Teesside University, Borough Road, Middlesbrough TS1 3BA, UK
[d] School of Life Sciences, University of Nottingham Medical School, Nottingham NG9 6HZ, UK
[e] Liverpool John Moores University, Liverpool, UK

ARTICLE INFO

Keywords:
Second-harmonic generation microscopy
Collagen type I
FTIR
Raman spectroscopy
Ancient bone

ABSTRACT

Second-harmonic generation imaging (SHG) captures triple helical collagen molecules near tissue surfaces. Biomedical research routinely utilizes various imaging software packages to quantify SHG signals for collagen content and distribution estimates in modern tissue samples including bone. For the first time using SHG, samples of modern, medieval, and ice age bones were imaged to test the applicability of SHG to ancient bone from a variety of ages, settings, and taxa. Four independent techniques including Raman spectroscopy, FTIR spectroscopy, radiocarbon dating protocols, and mass spectrometry-based protein sequencing, confirm the presence of protein, consistent with the hypothesis that SHG imaging detects ancient bone collagen. These results suggest that future studies have the potential to use SHG imaging to provide new insights into the composition of ancient bone, to characterize ancient bone disorders, to investigate collagen preservation within and between various taxa, and to monitor collagen decay regimes in different depositional environments.

1. Introduction

The collagen fraction of ancient bones holds historical information related to bone taphonomic history, and even holds some biological information about ancient life. Analyses of ancient bone collagen have included collagen extraction for radiocarbon dating, weight measurement, stable isotope analyses, and sequencing. These techniques investigate research problems such as emplacement ages (Arslanov and Svezhentsev, 1993), collagen decay regimes (Buckley et al., 2008), paleodiets (Lee-Thorp et al., 1989), and cladistics analyses (Morvan-Dubois et al., 2003), respectively. Second-harmonic generation (SHG) imaging specifically targets type I collagen, without sample destruction. It has contributed significantly to biomedical research on collagen structures (Mohler et al., 2003) and diseases through imaging tissues in vivo (Brown et al., 2003) and in modern bone (Chen et al., 2012; Ambekar et al., 2012), suggesting its potential to explore ancient bone. SHG imaging could supply new insights into the collagen composition of ancient bones, including disease characterization, extent and distribution of collagen, collagen decay characteristics, and preservation favorability of various decay environments.

1.1. Second harmonic generation imaging

SHG imaging takes advantage of the interaction between two low-energy photons with type I collagen present in bone. Collagen is structured such that it can absorb the two low energy incident photons and re-emit them as a single photon with twice the energy (frequency) at half the wavelength (Strupler et al., 2007). This non-invasive quality is attractive to biomedical researchers, since it does not require the addition of dyes such as fluorophores as does two-photon imaging that otherwise uses a very similar confocal microscope setup. Addition of dyes is not required to image collagen structure using SHG, thus protecting valuable specimens of ancient bone. Finally, two-photon and SHG imaging use low energy infrared laser light which does not burn live tissues. SHG thus appeals as a technique that captures collagen-specific images without disrupting labile biomolecular remnants endogenous to ancient bone.

Type 1 collagen fibres in fresh bone range from 0.3–3 μm thick (Naik et al., 2014). A fibre consists of a dozen or so packaged fibrils, each ranging from 10 to 300 nm. One fibril contains many assemblies of parallel, crosslinked, triple helical collagen molecules, each also called

* Corresponding author at: Department of Electrical Engineering & Electronics, Mass Spectrometry Research Group, University of Liverpool, Brownlow Hill, Liverpool L69 3GJ, UK.
E-mail addresses: brian.thomas@liv.ac.uk (B. Thomas), d.g.mcintosh@liv.ac.uk (D. McIntosh), tlf@liverpool.ac.uk (T. Fildes), lynnsmith@nortonpriory.org (L. Smith), frankhargrave@nortonpriory.org (F. Hargrave), m.islam@tees.ac.uk (M. Islam), T.Thompson@tees.ac.uk (T. Thompson), robert.layfield@nottingham.ac.uk (R. Layfield), daniel.scott@nottingham.ac.uk (D. Scott), barry.shaw@nottingham.ac.uk (B. Shaw), c.l.burrell@2009.ljmu.ac.uk (C.L. Burrell), S.Gonzalez@ljmu.ac.uk (S. Gonzalez), s.taylor@liv.ac.uk (S. Taylor).

http://dx.doi.org/10.1016/j.bonr.2017.10.005
Received 16 June 2017; Received in revised form 27 September 2017; Accepted 24 October 2017
Available online 01 November 2017

tropocollagen. During degradation, collagen fibres essentially fray and disperse into their smaller components. Confocal microscopy used for SHG imaging can resolve fully formed type 1 collagen fibres, but leave fibrils and tropocollagen too small for SHG to detect even though they could remain in bone as protein remnants. SHG thus has the potential to nondestructively characterize bone collagen fibre morphology and its decay patterns over time and across various environments. Further, there is evidence that in certain bone diseases (e.g. Paget's disease), defects in molecular rearrangements of collagen type I like beta-isomerization may occur (Cloos et al., 2003), and the prospect of applying SHG to study such disorders in archaeological bone samples also remains to be explored.

1.2. SHG imaging and protein verification in ancient bones

Various techniques can be used to determine (and in some cases quantify) the presence of endogenous organics in bone. Raman spectroscopy reveals vibrational modes of characteristic molecular arrangements, including the amide bond (Penel et al., 2005). Similarly, Fourier transform infrared spectroscopy (FTIR) reveals absorption spectra characteristic of protein chemical structure (Gu et al., 2013). Protein sequences derived by tandem mass spectrometry can be matched to primary structural data in databases that include microbe versus vertebrate protein sequences as a test against exogenous protein sourcing. The physical extraction and weighing of the collagen bone fraction during sample preparation for radiocarbon dating by AMS inadvertently but directly verifies the presence of primary collagen in ancient bone. In this study we used the above four techniques to test the hypothesis that SHG can detect collagenous remnants in ancient bones from various ages, taxa, and settings. SHG imaging is thus established as an important new tool to explore specific questions about how various burial environments and histories may have influenced collagen decay patterns in different ancient bones.

2. Materials and methods

2.1. Sample descriptions

2.1.1. Geography and stratigraphy

Eight bone samples of known provenance were obtained to test the potential of SHG imaging to supply novel information about collagen type I in ancient bone from multiple localities, ages, and depositional environments. Described in more detail below, these included a modern bovine femur used as a reference. Five samples including three human (NP71_12_9, NP71_13_9, NP73_34_81) and two bovine (NP77_109_5, NP77_109_34) came from one of Europe's most excavated sites, Norton Priory, UK. Additionally, a Pleistocene *Megatherium americanum* ilium fragment (EHRC90002) from California's Northern Sacramento valley and a well-weathered Pleistocene camelid from Oregon test SHG's utility on much older bones and on sedimentary as opposed to burial settings.

Norton Priory, a historic Augustinian monastery in Cheshire, UK, included an ancient abbey active from its foundation in 1134 CE to the 16th century. Recent analysis of human burial remains excavated there beginning in the 1970s found an abnormally high incidence of skeletons affected by a disorder resembling Paget's disease of bone (Burrell et al., 2016). Paget's disease is a focal disorder characterized by disorganized histological bone structure sometimes accompanied by abnormal curvature of limb bones, especially including the femur (Aaron et al., 1992). An affected human left ulna (NP71_12_9), a rib fragment (NP73_34_81) from skeleton 101 (SK 101) and a right fibula (NP71_13_9) were selected from burials excavated in 1971 and 1973. Sample NP71_12_9 belongs to Skeleton 35, Grave 34 and sample NP73_34_81 belongs to Skeleton 101, Grave 116. AMS radiocarbon dating was successful for these individuals. The 2 σ results for Skeleton 35 presented a single date of Cal 1155–1260 CE (Cal BP 795–690) whereas Skeleton 101 presented two possible dates; Cal 1280–1320 CE (Cal BP 670 to 630) and Cal 1350–1390 CE. AMS radiocarbon dating of sample NP71_13_9, belonging to Skeleton 29, Grave 28 was unsuccessful. However, it has been estimated that this burial is from the late 14th Century (i.e. also medieval) based on the surrounding archaeology. All individuals are male and over 45 years of age. Disease-affected, as opposed to unaffected, bones were not necessary for this study but were included for two reasons. First, they were available to our group as bones from which collagen was confirmed by extraction for radiocarbon dating. Second, they illustrate the potential for future studies to implement SHG imaging as a novel means to characterize ancient bone disease.

A bovine tibia (NP77_109_5) and a bovine radius (NP77_109_34), were both excavated in 1977 from an associated midden-like deposit. Portions of each were sacrificed for radiocarbon analysis. The collagen fraction of NP77_109_5 was AMS radiocarbon (2 σ) dated to Cal 1300–1360 CE or 1380–1420 (Cal BP 650–590 or 570–530) due to two intersections of the mean radiocarbon age with the calibration curve. The collagen fraction of NP77_109_34 was AMS radiocarbon dated to Cal 1027–1161 CE (Cal BP 923–829; 2 σ). The bioapatite fraction of NP77_109_34 was radiocarbon dated by AMS to BP 860 ± 20 (not calibrated; corresponding before calibration to 1070–1110 CE). Table 1 summarizes these ages in years before present (CalBP), i.e. years before 1950, calibrated. These bovine bones explore the capacity of SHG to reveal information from unintentionally buried bones, for example how their differential diagenesis may have affected their collagen content and distribution.

The Pacific Gas Transmission/Pacific Gas and Electric (PGT-PG&E) Pipeline Expansion Project conducted in the western US during 1993–1994 contained guidelines requiring the collection and preservation of any fossils encountered while trenching over 800 miles. One of the project's largest and most complete fossils consisted of a partially complete *Megatherium* (ground sloth) taken from the Pleistocene Red Bluff Formation of Colusa County, California. Another, better-preserved Project find was an ancient camelid from the upper Pleistocene Palouse Formation in Oregon. All pipeline fossils are housed

Table 1
Radiocarbon results.

Description	^{14}C age bp (collagen)	^{14}C age bp (apatite)
Bovine tibia NP77 109 5	573 ± 23 (QUBC-24093)	
Bovine radius NP77 109 5	570 ± 30 (Beta-368,271)	
Bovine radius NP77 109 34	934 ± 30 (QUBC-24091)	860 ± 20 (UGAMS-17385)
Human left ulna NP71 12 9	840 ± 30 (Beta-425,286)	
Human rib NP73 34 81	660 ± 30 (Beta-425,288)	
Camelid fragment EHRC90001	12,060 ± 89 (AA-106299)	10,170 ± 30 (UGAMS-20474)
Megatherium femur EHRC90002		20,050 ± 40 (UGAMS-20475)

NP = Norton Priory; EHRC = Earth History Research Center; QUBC = Queen's University Belfast (CHRONO); Beta = Beta Analytic; UGAMS = University of Georgia Accelerator Mass Spectrometer (Center for Applied Isotope Studies); AA = University of Arizona (Accelerator Mass Spectrometry Lab). *Skeleton 35, Grave 34, excavated 1971, included Pagetic human left ulna NP71 12 9 as described elsewhere in this report.

at the permanent repository of the Earth History Research Center (EHRC) in Keane, Texas. A thumb-sized fragment that had already fallen from the mostly intact camelid (EHRC90001) limb bone was sectioned for SHG imaging. Its collagen fraction was AMS radiocarbon dated by the University of Arizona to 12,060 ± 89, CalBP. These Pleistocene samples explore the age range of samples that SHG can image, as well as differences between SHG and other methods (such as FTIR and physical extraction) of quantifying collagen remnants. Comparison of primary bone collagen structure from modern, medieval, and ice age bones demonstrates the applicability of SHG imaging to ancient bones varied biological and taphonomic origins.

2.1.2. Radiocarbon dating

Radiocarbon dating of bone samples was performed using four different commercial laboratories: Queen's University Belfast (CHRONO), Beta Analytic, University of Georgia Center for Applied Isotope Studies, and the University of Arizona's Accelerator Mass Spectrometry Lab. Sample preparations including acid demineralization pretreatments had slight differences, but used the industry standard acid-alkali-acid (AAA) strategy to extract and gelatinize collagen. *Megatherium* EHRC90002 had insufficient collagen for radiocarbon analysis, so the radiocarbon from the bone bioapatite was measured instead, and used to compare with two other bioapatite-derived radiocarbon ages from our small bone set. The purpose of the present study does not include precision archaeological timing of emplacement for the samples under consideration. Instead, radiocarbon results are here used primarily to confirm the presence of endogenous proteins via physical collagen extraction and secondarily to illustrate how future research on time-stamped ancient bone could benefit from SHG imaging results.

2.2. Second harmonic generation imaging

2.2.1. Sample preparation for SHG

Bone was initially sectioned by hand saw. Samples with a length of approximately 1.5 cm, measured along the axial orientation, were cross-sectioned using a Buehler Isomet low-speed saw fitted with a circular diamond-tipped blade. Bone slice thicknesses of approximately 300 μm were targeted. However, ancient bone proved brittle and fragile, resulting in some uneven wedge-shapes and non-level surfaces. Slices were mounted on glass slides. Images were collected before and after a 20 min bath in 10% acetic acid to test whether or not acid would etch biominerals to expose protein to improve SHG visualisation.

2.2.2. Second harmonic generation apparatus

SHG imaging was performed using a dedicated two-photon confocal microscope assembly at the Live Cell CORE Imaging facility at the University of Texas Southwestern Medical Center in Dallas. Mounted bone samples were imaged with a Zeiss Plan-Apochromat 10×, NA = 0.45 objective lens using a Zeiss Examiner Z1 two-photon excitation laser scanning confocal microscope (Carl Zeiss, Jena, Germany) coupled to a Coherent Chameleon titanium:sapphire laser (Coherent, Glasgow, UK). The laser was set to 920 nm for excitation. Laser power at the specimen was approximately 13 mW. SHG emissions were collected from 420 to 480 nm, and autofluorescence emissions were collected from 500 to 550 nm with band-pass filters mounted in a standard P&C filtercube. The SHG emission signal was collected at 458 nm (half the incident wavelength) and a parallel autofluorescent signal was collected at 760 nm using a dual channel Zeiss LSM BiG detector. The BiG can collect images at different wavelengths simultaneously. Autofluorescence reveals cellular components that include various lipopigments and vitamin derivatives (Zipfel et al., 2003) as well as aromatic amino acids (Monici, 2005) useful for comparison with collagen distribution within bone. Focal planes and bone regions were selected to include sufficient collagen to visualise within the viewing frame. Frame sizes of 1932 × 1932 pixels were rastered at 5 s speed, taking the average of 4 reads per line. Fig. 1 shows composite images of SHG in red, merged with autofluorescence in green, discussed below.

Zeiss Efficient Navigation (ZEN) software proprietary to the microscope system was used to control equipment and capture raw images in .czi file format. Open source ImageJ software package Fiji (Schindelin et al., 2012) was used to process the data, which included merging the channels and adjusting channel brightness, to produce Fig. 1. Pixel intensity from each channel (458 and 760) ranged from 0 to 255. An intensity threshold of 75 was used for both channels to maximize collagen and organic signals against the background. After merging red and green channels, the brightness ranges were adjusted to balance disparate intensities from the two channels. For example, modern bone had so much collagen that its red SHG signal overwhelmed the autofluorescence. Therefore its hues were set to 40–255 to dim the powerful SHG signal enough to visualise autofluorescence, as shown in Fig. 1A. Older bones had dramatically less collagen content and hence dramatically dimmer SHG than autofluorescent signals. Therefore, hues from Medieval and ice age bone samples were set from 20 to 255 to enhance the red SHG signal from faint collagen traces.

2.3. Raman spectroscopy

Raman spectroscopy reveals vibrational and rotational modes of various covalent bonds, which raise or lower the energy level of laser light. It has been used to characterize amide bonds in collagen (Gullekson et al., 2011). Raman spectra from five ancient bones and one modern bovine bone were collected at the Laboratory of Imaging Mass Spectrometry at the University of North Texas (UNT) in Denton. A Horiba iHR550 Imaging Spectrometer was set to full scan range of 200–2600 cm^{-1}. The instrument was calibrated every fourth scan.

2.4. Fourier transform infrared spectroscopy

FTIR spectroscopy of medieval bovine tibia NP77_109_5, ice age *Megatherium americanum* EHRC90002, and one modern bovine bone was performed at the School of Science and Engineering, Teesside University. A Perkin Elmer Spectrum 100 FTIR spectrometer with a diamond attenuated total reflectance (ATR) accessory was used to make measurements. A few mg of bone from each sample was ground with an agate mortar and pestle and then placed in contact with the ATR accessory. The SPECTRUM™ software was used to record spectra over the wavelength range 650 cm^{-1} to 2000 cm^{-1} at a spectral resolution of 4 cm^{-1}. Each spectrum was an average of 16 scans.

The ratio of the main amide peak height to the phosphate peak height represents relative amounts of collagen to bioapatite in a bone sample. Since collagen decays, its peak height should decrease over time. To confirm collagen decayed in ancient bone, FTIR spectra shown in Fig. 3 were collected from three bone samples representing modern, Medieval, and ice age time frames. All three bones were used in multiple, overlapping collagen detection techniques as described below. The degree of collagen preservation was estimated by calculating the ratio of protein-specific amide bond stretching to bioapatite-specific phosphate stretching as per Thompson et al. (2013, 2009). The carbonyl stretch of the amide bond in collagen generates a spectral peak height at 1650 cm^{-1}, and the phosphate stretch of the apatite fraction in bone generates a peak at 1035 cm^{-1}. A higher value of the carbonyl-to-phosphate peak height ratio (carbonyl/phosphate, or CO/P) corresponds to better collagen preservation.

2.5. Protein extraction and sequencing

Protein extraction from ancient bone for mass spectrometry-based sequencing (LC-MS/MS) proceeded according to the method of Jiang et al. (2007). Briefly, bone powder (~50 mg; NP73_34_81; medieval human rib) was demineralized (1.2 M HCl) and then incubated sequentially with extract buffer 1 (100 mM Tris, 6 M Guanidine-HCl, pH 7.4), extract buffer 2 (100 mM Tris, 6 M Guanidine-HCl, 250 mM

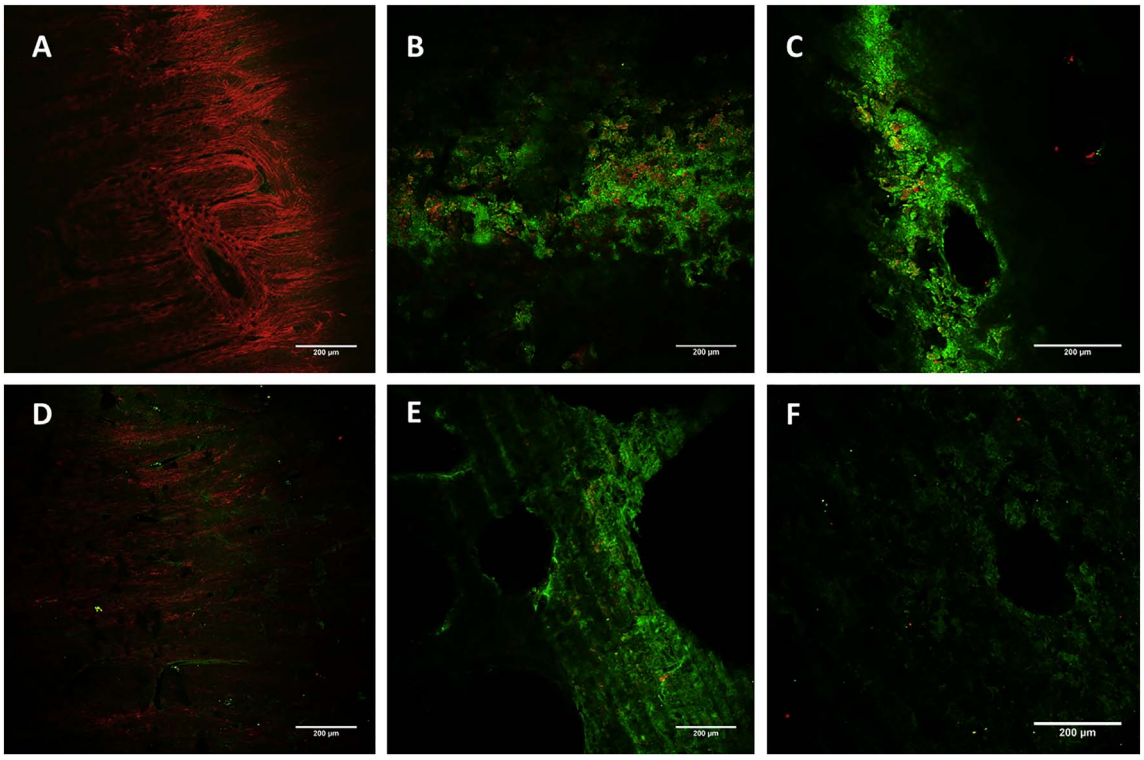

Fig. 1. Second-Harmonic Generation (SHG) images of six bones.
Collagen SHG detection is shown in red, and the green shows autofluorescence of mostly organic, non-collagen bone tissue constituents. The SHG (red) signal generally diminishes with older bones, consistent with collagen decay over time. This sample set shows that SHG reveals collagen in a wide range of taxa, ages, and settings. The scale bars equal 200 µm. The brightness range for both red and green channels was set to 0–75. **A**) A cross-section of cortical bone from the proximal diaphysis of modern bovine femur shows dense collagen bands that encircle osteons. **B**) The uneven surface of a thin section of Medieval human rib bone NP73_34_81 (SK101) from Norton Priory, UK reveals significant collagen decay relative to modern bone, as well as irregular collagen deposition, presumably due to Paget's disease. **C**) Red collagenous remains in Norton Priory Pagetic human left ulna NP71_12_9 (SK 35) were confirmed by protein sequencing (see text). **D**) Norton Priory bovine tibia NP77_109_5 cortical bone shows better collagen signal than the two human samples B and C, possibly because of Paget's effect on postmortem bone decay, or differences between human burial versus trash deposition. **E**) Upper Pleistocene Camelid EHRC9001 from Oregon, USA shows barely visible collagenous remnants. **F**) Pleistocene *Megatherium* ilium EHRC90002 from California, USA shows the least collagen signal among the bones under consideration here. (For interpretation of the references to color in this figure legend, the reader is referred to the web version of this article.)

EDTA, pH 7.4) and finally 6 M HCl. Following each extraction step, the bone powder was pelleted by centrifugation (16,000*g* for 10 min at 4 °C) and washed in deionised water. The supernatant was discarded, with the exception of the 6 M HCl extract, which was utilised in subsequent analyses; either probed directly by SDS-PAGE using a 5–20% polyacrylamide gradient gel (visualised with silver-staining), or taken forward to MS/MS analysis.

For the latter the 6 M HCl extract was digested with trypsin according to a modified FASP strategy, with subsequent LC-MS/MS analysis carried out using an RSLC nano-HPLC system (Dionex, UK) and an LTQ-Orbitrap-Velos mass spectrometer (Thermo Scientific) essentially as detailed by Scott et al. (2016). The .raw data file obtained from the LC-MS/MS acquisition was processed using Proteome Discoverer (version 1.4.0.288, Thermo Scientific), with the file searched using Mascot (version 2.2.04, Matrix Science Ltd.) (Perkins et al., 1999) against the UniprotHuman_2015_02 database (unknown version, 67,911 entries) assuming the strict trypsin digestion. The peptide tolerance was set to 10 ppm and the MS/MS tolerance was set to 0.02 Da. Fixed modifications were set as alkylation of cysteine, and variable modifications set as deamidation of asparagine and glutamine, and oxidation of methionine and proline residues. Scaffold Q + S (Searle, 2010) (version 4.4.1.1, Proteome Software) was used to validate MS/MS based peptide and protein identifications from Proteome Discoverer. Peptide identifications were accepted if they could be established at greater than 95.0% probability, with a minimum of two peptides required for protein identification.

3. Results and discussion

3.1. SHG imaging captures faint signals in ancient bone

Before use of SHG imaging as a diagnostic technique for research questions pertaining to ancient bones from various settings, taxa, and ages, it first needs to be shown that the methodologies used here can reliably image the same bone component—namely collagen type 1—in modern as in ancient bone. The first step to establish this was to capture SHG images from bone samples from different settings and ages and compare them with modern bone. Fig. 1A shows typical collagen-dense (colored red) modern bovine cortical bone. Roughly concentric striated collagen fibres, perforated by small black patches that correspond to osteocyte lacunae, wrap around oval-shaped osteons. This result conforms to other SHG images of modern bone (Schrof et al., 2014). Fig. 1B–F show SHG images of ancient bones and permit, for the first time, comparison with modern bone. In all five ancient samples, the red SHG signal is greatly reduced compared to modern bone. We performed subsequent analyses to verify that these red traces correspond to primary (i.e. endogenous) and not contaminating, bone collagen.

Uneven autofluorescence patterns, particularly evident in Fig. 1B (Human rib NP73_34_81) and 1C (Human left ulna NP71_12_9), do not reflect structures inherent to the bone, but rather uneven surface samples and regions where the focal plane captured slanted surfaces. This became evident when focusing up or down brought higher or lower regions into focus. Acetic acid pretreatments of bones for image resolution improvement were inconclusive, so the application of acetic acid to bone surfaces was discontinued. Medieval human, Medieval

bovine, and Pleistocene *Megatherium* bone all show at least faint collagen traces, visible as red blotches and dots. We conclude that these represent collagenous remnants for three reasons. Firstly, the diminishing signal with increasing age generally corresponds to established collagen decay regimes as described below. Secondly, separate techniques verify protein within our bone samples, as described in the next section. Thirdly, literature consistently reports significant contributions to SHG signal from collagen type 1, which has been firmly established as the primary source in modern bone.

The hue range of 20 to 255 was chosen to strike a balance between the two channels so that each image includes both the collagen and autofluorescent signals. The same hue range was applied to all ancient bone images, but not modern bone, to equally compare collagen content across samples from a variety of burial settings and ages. Visual inspection reveals a loss of collagen signal strength over time. The three Medieval bones shown in Fig. 1B–D all have more collagen than the two Pleistocene bone shown in Fig. 1E and F. In addition, Fig. 1D shows a bovine bone of roughly the same age as the two human bones in Fig. 1B and C. These should show a similar concentration of collagen if time is the sole factor in collagen decay. However, the bovine bone shows a higher collagen concentration, possibly due to diagenetic differences between intentional burial of humans versus the midden-like setting of the discarded bovine bone.

Future studies can use SHG images of ancient bone to quantify collagen using the signal area in a single image, as per Chiu et al. (2010) who calculated a collagen area ratio (CAR) by dividing the pixels of interest (collagen) by those presumed to represent the total organic area (for example, autofluorescent pixels). Alternatively, future studies could quantify collagen volume by subtracting collagen signal from organics in 3-D rendered z-stacks like that shown below. Future studies could combine either strategy with radiocarbon or otherwise age-dated bone samples to explore collagen decay regimes in specific settings. More research will also be necessary to determine if enough collagen remains in Medieval human bones for SHG imaging to reveal disease affected or non-affected patterns.

Despite the positive identification of collagen using SHG, faint permineralisation caused slight darkening of the outermost 1.5 mm of the Pleistocene camel cortical bone EHRC90001. Dark, microscopic flecks of mineral within the bone appeared as red block shapes under SHG. Regions deeper within the original bone than about 3 mm had no dark flecks and no red block shaped signals, but they did have the same red blotches characteristic of collagenous remnants in all samples within this study. This result showed that although SHG signals can reveal collagen in ancient bone, they can also reveal mineralization, suggesting that discernment of bone microstructure and decayed collagen morphologies, and not color alone, will be important for workers to qualify ancient bone collagen using SHG.

3.2. Four techniques confirm protein in SHG-imaged ancient bone samples

Raman spectra of these ancient bones shown in Fig. 2 revealed broad shoulders instead of the sharp corresponding peaks from modern. As proteins hydrolyze and/or cross-link through diagenetic alteration and decay, and as their concentrations diminish, many of their corresponding Raman peaks lose distinctiveness of shape. Morris and Finney (2004) identified the Raman spectral peak near 1340 wavenumbers (in cm^{-1}) in modern bone as an amide III vibrational mode, and the Raman spectral peak near 1530 cm^{-1} as an amide II vibrational mode. Fig. 2 shows sharp amide peaks from modern bovine bone (blue spectrum) that indicate strong protein bond vibrations. The two ancient bone spectra include human bone NP77_109_5 to represent a typical Raman spectrum from our Medieval bone set (purple spectrum) and *Megatherium* bone EHRC90002 to represent an ice age sample. These decreased amide bonds in ancient bones include shoulders and shallow peaks relative to modern bone. The shifts in ancient bone spectral shoulders toward higher wavenumbers than the peak values from modern bone are attributed to postmortem chemical alterations. Peak height reductions over time were also observed, consistent with McLaughlin and Lednev's measured Raman peak reductions especially in the CH_2 region of turkey bone buried for 68 days (McLaughlin and Lednev, 2011). These results are consistent with diminished primary bone protein such as collagen.

FTIR in conjunction with Raman spectroscopy has been used to assess collagen quality in archaeological samples, and even to prescreen samples suitable enough for radiocarbon analysis (Boaretto et al., 2009). FTIR has also been used to characterize amino acids and amide bond signatures from blood vessel-like remains from fossils as deep as Triassic (Surmik et al., 2016). A similar technique confirmed the left-handed triple helical configuration indicative of collagen in a Jurassic sauropod rib bone (Lee et al., 2017). These demonstrate the sensitivity of the FTIR technique to detect proteinaceous signatures when applied to ancient bone samples that have been sufficiently well preserved. The blue FTIR spectrum in Fig. 3 corresponds to the same modern bone used for Raman spectroscopy (blue spectrum in Fig. 2) and SHG image (Fig. 1A). Likewise, the purple FTIR spectrum in Fig. 3 shows NP 77_109_5, the same Medieval bone as the purple Raman spectrum in Fig. 2. The green spectra in both Fig. 3 and Fig. 2 show amide bond vibration in Pleistocene camel EHRC 90002. Additionally, collagen was extracted for successful radiocarbon dating from both NP77_109_5 and EHRC 90002. Finally, Fig. 1D shows collagen in the SHG image of NP77_109_5, and Fig. 1F shows small traces of collagen (in red) within the SHG image of EHRC 90002. Fig. 3 compares modern bovine (blue spectrum) with medieval bone (purple, bovine tibia NP 77_109_5) FTIR spectra. The carbonyl peak at $\sim$1650 cm^{-1} indicates reduced but preserved collagen in the Medieval sample. The Pleistocene sample (green spectrum in Fig. 3) is further reduced from the Medieval, again consistent with collagen loss due to decay over time.

Table 2 shows the carbonyl and phosphate FTIR peaks used to calculate CO/P ratio for the three bones in Fig. 3.

These calculations confirm what Fig. 3 also reveals: a decrease in CO/P ratios with older bone samples. This decreased collagen signal, similar to those decrease signatures seen in Raman spectra peaks that develop shoulders with age (Fig. 2) and SGH signal weakening with age (Fig. 1), are consistent with artificial protein decay experiments that show bone collagen decay matching a first-order, temperature-dependent model while hydrated (Collins et al., 1995) and confirm that these bones retain endogenous proteinaceous content.

Protein extraction from the SHG-imaged medieval human rib sample (SK 101) was confirmed by SDS PAGE analysis, which demonstrated a characteristic protein 'smear' [Fig. 4A] consistent with the presence of collagens. Mass spectrometry-based protein sequencing revealed remarkable collagen preservation seven centuries post-burial, and identified numerous peptide sequences corresponding to human collagen alpha-I (COL1Al, 59% sequence coverage) and collagen alpha-II (COL1A2, 65% sequence coverage) [Fig. 4B, C], representing both chains of collagen type I, and entirely consistent with the SHG data.

The sample preparation process for radiocarbon dating inadvertently also provides evidence for endogenous collagen remnants in ancient bone. Table 1 summarizes eight radiocarbon results from six ancient bones with varying degrees of collagen-indicating SHG signal. Three different radiocarbon dating laboratories found sufficient fractions of insoluble collagen in five of six bones. The *Megatherium* (EHRC90002) bone had insufficient collagen for radiocarbon dating, consistent with the small traces of SHG signal seen in Fig. 1F. Typical cutoff fractions for commercial radiocarbon laboratories equal approximately 1% by weight collagen/total bone (Brock et al., 2012). Fig. 1 includes SHG images of two (tibia NP77_109_5, and EHRC90001) of the five bones shown in Table 1 that contained sufficient collagen for radiocarbon analysis. One bone sample (Bovine radius NP77_109_5) was selected for a z-stack of SHG images, and is shown in Fig. 5.

In summary, results from four independent techniques verify primary protein in our ancient bone set. These results are consistent with

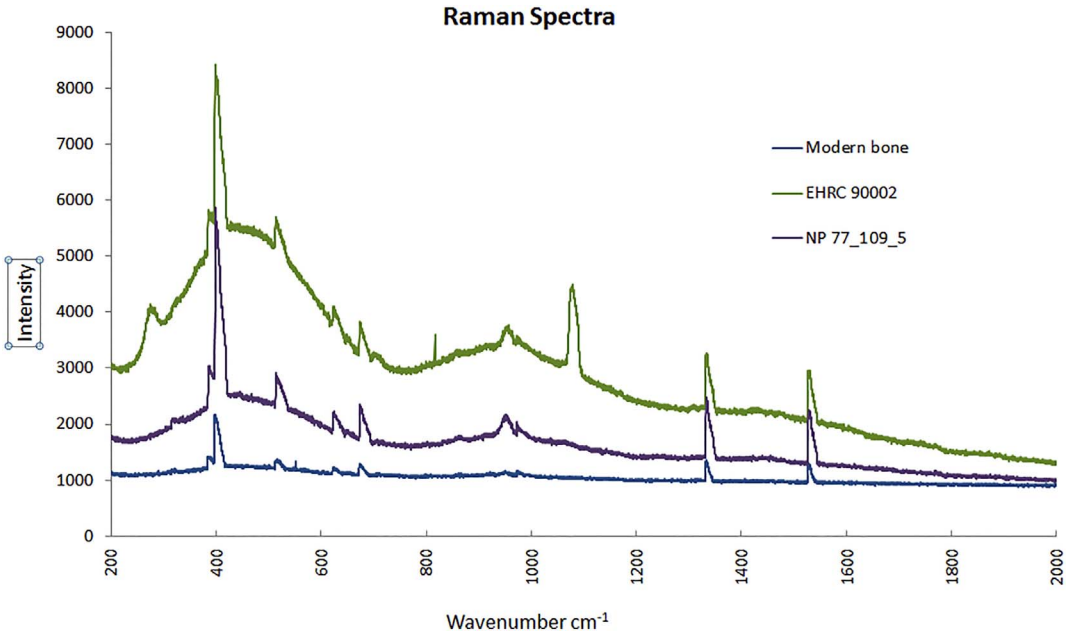

Fig. 2. Raman spectra of bone collagen amide peaks.
Modern bovine, Medieval bovine, and Pleistocene *Megatherium* bones show corresponding bone collagen amide III vibrational mode peaks near 1340 cm^{-1}, and amide II peaks near 1530 cm^{-1}. Peak heights appeared to diminish in the Pleistocene but not the medieval sample. Peak wavenumbers decreased slightly with age.

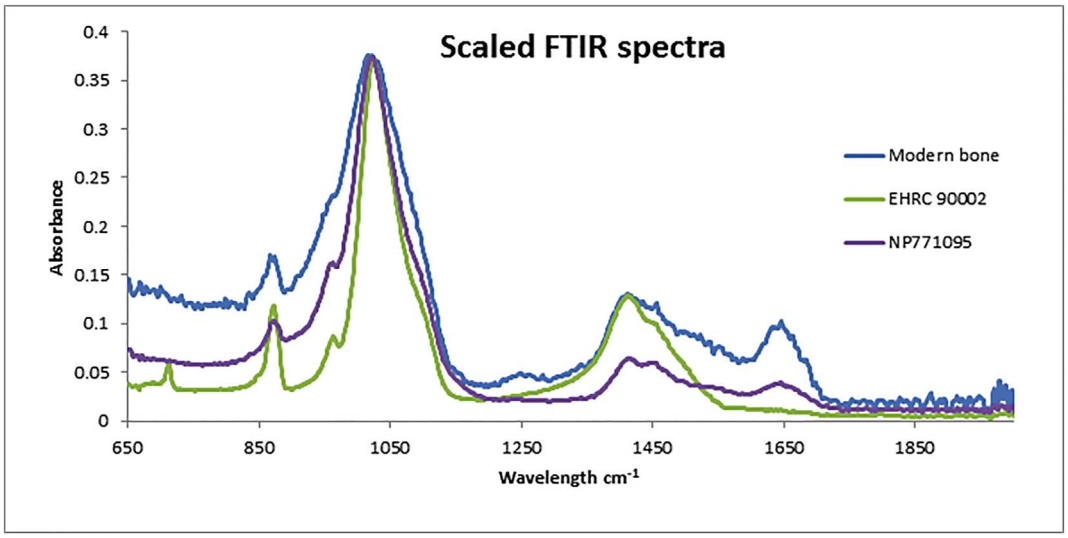

Fig. 3. FTIR spectra of three bones show collagen decay.
Modern, Medieval, and Pleistocene bones each show collagen-based carbonyl (CO) stretch peaks near 1650 cm^{-1}. These peaks decrease with age, indicating protein loss. The phosphate (P) peak at 1035 cm^{-1} stays relatively stable over time, enabling a calculation of the CO/P (essentially collagen/bioapatite) ratio as shown in Table 2.

Table 2
Carbonyl and phosphate FTIR peak values.

Bone source:	Modern	Medieval (MNP77_109_5)	Ice Age (EHRC90002)
P (1025 cm^{-1})	0.0533	0.2212	0.3707
CO (1650 cm^{-1})	0.0136	0.0217	0.0132
CO/P =	0.26	0.10	0.03

the hypothesis that SHG imaging of ancient bone detects decayed remnants of original bone collagen. Raman spectroscopy, FTIR spectroscopy, and SHG imaging all probe the chemical makeup of bone samples without the need to treat or destroy the sample. Standard radiocarbon bone sample pretreatments and protein sequencing bone sample preparations destroy small amounts of the artefacts, but they firmly secure the presence of endogenous ancient bone proteins.

3.3. 3-D SHG imaging of ancient bone

By recording SHG images at different focal planes a z-stack of images from bovine radius NP77_109_5 was collected. 75 planar SHG images, each measuring 1214 × 1214 μm, spanned a depth of 750 μm to provide a resolution of 10 μm in the z-axis. Bitplane (Oxford Instruments) Imaris image analysis software was used to collate the stack into a 3-D model (Fig. 5A) and to render the z-stack in 3-D and apply a space-filling model to both channels. As in all Fig. 1 images, the red represents collagen and green represents autofluorescence, both shown in Fig. 5A. Fig. 5B renders the green autofluorescence channel, which indicates the presence of proteinaceous and lipid residues, as a space-filled model to against which the smaller SHG signal in order to illustrate the spatial positioning of collagen remnants shown in red. The red signals in Fig. 5 indicate remnants of bone collagen type 1. SHG in

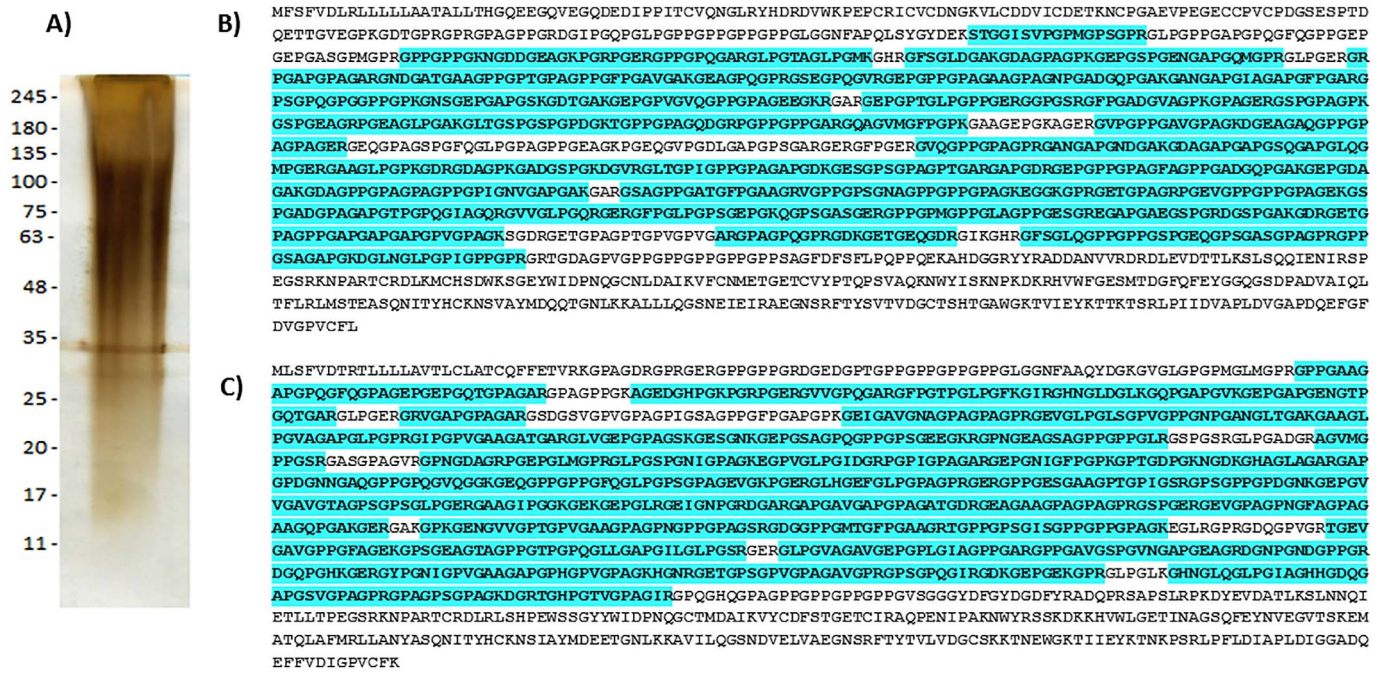

Fig. 4. Collagen sequence in Medieval human rib bone NP73_34_81 (SK 101).
A) SDS PAGE of ~700-year-old human bone protein extract still shows a visible protein smear, consistent with endogenous collagens. **B**) SK 101 had a 59% sequence coverage of the human collagen alpha-I chain. **C**) SK 101 had a 65% sequence coverage of the human collagen alpha-II chain.

bone loses resolution with depth, and did not work well beneath 1 mm. However, Fig. 5 suggests that future SHG studies can nondestructively probe for collagen almost 1 mm beneath the exposed surface of an ancient bone sample. SHG images from additional bone samples representing more continuously graded ages could reveal post-mortem type I collagen decay patterns, and images from diseased versus normal human bone could further characterise bone health in ancient populations.

4. Conclusion

Four separate protein detection techniques confirm the presence of proteinaceous organic remains in the same ancient bones from which SHG imaging captured signals consistent with endogenous collagen type I. We conclude that it is possible to visualise the distribution of tiny patches of collagen in ancient bone using SHG imaging. Our results further demonstrate that SHG imaging reveals bone collagen remnants in a wide (modern to Pleistocene) age range, which additional research could potentially expand. Finally, SHG images of Medieval bone collagen show variation in collagen preservation even from a single location (Norton Priory), suggesting its potential to explore causes of differential collagen preservation. However, collagen-like SHG signals from exogenous minerals caution that experiential knowledge of bone microstructure including collagen remnant morphologies is necessary (without the assistance of other techniques) to discern collagen in partly mineralised ancient bone. Future work can leverage digital image

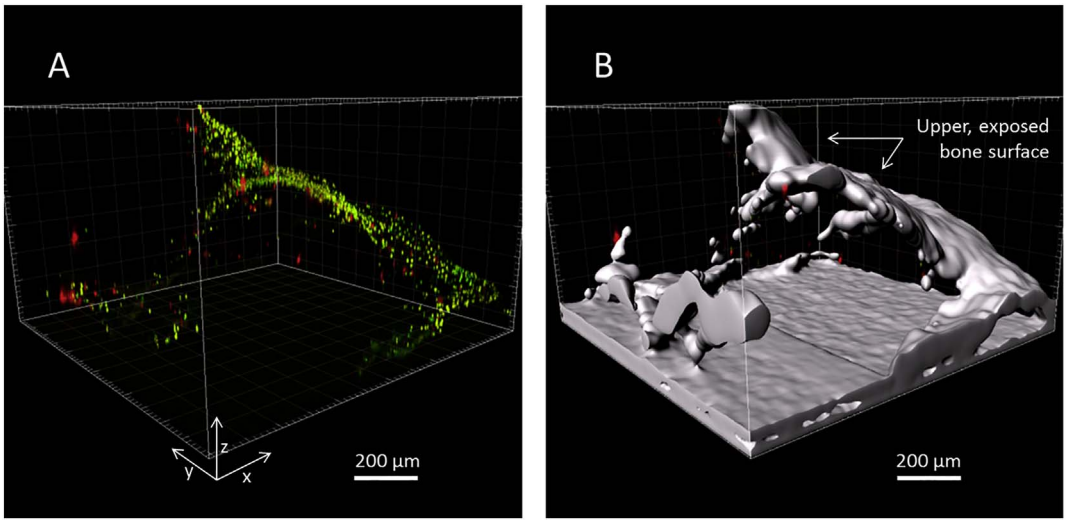

Fig. 5. SHG z-stack reveals 3-D distribution of collagen in ancient bone surface.
Medieval bovine radius NP77_109_5, radiocarbon-dated to approximately 1380 CE, shows faint collagenous remnants colored red. Areas with no color represent trabecular spaces. 75 2-D images spaced 10 µm apart spanned a depth of 750 µm, totaling a 1 mm × 1 mm × 0.75 mm volume. **A**) Stacked 3D image with red SHG that shows collagen remnants and green autofluorescence that shows other organics (see text). **B**) Imaris software was used to render a solid grey space-fill function around the green signal to reveal non-overlapping collagenous volumes. (For interpretation of the references to color in this figure legend, the reader is referred to the web version of this article.)

processing of SHG data to estimate collagen content and visualise the 3-D distribution of collagen in ancient bone surfaces up to 1 mm deep. SHG imaging holds promise as a novel and nondestructive technique to investigate collagen in ancient bones of various settings, taxa, and ages.

Acknowledgements

Protein sequencing was funded in part by the Wellcome Trust (ref. WT107720MA) and we wish to thank the Protein Nucleic Acid Chemistry Laboratory (PNACL), University of Leicester, UK, for assistance with LC-MS/MS analyses. The Live Cell Imaging lab at the University of Texas Medical Center in Dallas, including Kate Luby-Phelps, Dorothy Mundy, and Abhijit Bugde, deserve special thanks for SHG training and access to confocal equipment made available in part through NIH S10 RR029731-01. Philip Mach at the University of North Texas provided tutelage on Raman spectroscopy and Rob van T'Hof at UoL for assistance with bone sectioning. Arthur Chadwick granted access to EHRC fossils curated at Southwestern Adventist University. Norton Priory Museums Trust kindly provided samples and Q-Technologies funded radiocarbon analyses.

References

Aaron, J.E., Rogers, J., Kanis, J.A., 1992. Paleohistory of Paget's disease in two medieval skeletons. Am. J. Phys. Anthropol. 89, 325–331.
Ambekar, R., Chittenden, M., Jasiuk, I., Toussaint Jr., K.C., 2012. Quantitative second-harmonic generation microscopy for imaging porcine cortical bone: comparison to SEM and its potential to investigate age-related changes. Bone 50, 643–650.
Arslanov, K.A., Svezhentsev, Y.S., 1993. An improved method for radiocarbon dating fossil bones. Radiocarbon 3, 387–391.
Boaretto, E., Wu, X., Yuan, J., Bar-Yosef, O., Chu, V., Pan, Y., Liu, K., Cohen, D., Jiao, T., Li, S., Gu, H., Goldberg, P., Weiner, S., 2009. Radiocarbon dating of charcoal and bone collagen associated with early pottery at Uychanyan Cave, Hunan Province, China. PNAS 106, 9595–9600.
Brock, F., Wood, R., Higham, T.F.G., Ditchfield, P., Bayliss, A., Ramsey, C.B., 2012. Reliability of nitrogen content (%N) and carbon:nitrogen atomic ratios (C:N) as indicators of collagen preservation suitable for radiocarbon dating. Radiocarbon 54, 879–886.
Brown, E., McKee, T., diTomaso, E., Pluen, A., Seed, B., Boucher, Y., Jain, R.K., 2003. Dynamic imaging of collagen and its modulation in tumors in vivo using second-harmonic generation. Nat. Med. 9, 796–800.
Buckley, M., Walker, A., Ho, S.Y.W., Yang, Y., Smith, C., Ashton, P., Oates, J.T., Cappellini, E., Koon, H., Penkman, K., Elsworth, B., Ashford, D., Solazzo, C., Andrews, P., Strahler, J., Shapiro, B., Ostrom, P., Gandhi, H., Miller, W., Raney, B., Zylber, M.I., Gilbert, M.T.P., Prigodich, R.V., Ryan, M., Rijsdijk, K.F., Janoo, A., Collins, M.J., 2008. Comment on “protein sequences from mastodon and Tyrannosaurus rex revealed by mass spectrometry.”. Science 319, 33c.
Burrell, C.L., Gonzalez, S., Smith, L., Emery, M.M., Irish, J.D., 2016. More than meets the eye: Paget's disease within archaeological remains. Am. J. Phys. Anthropol. 159, 105–106.
Chen, X., Nadiarynkh, O., Plotnikov, S., Campagnola, P.J., 2012. Second harmonic generation microscopy for quantitative analysis of collagen fibrillar structure. Nat. Protoc. 7, 654–669.
Chiu, Y.-W., Lo, M.T., Tsai, M.-R., Chang, Y.C., Hsu, R.-B., H-Y, Yu, Sun, C.-K., Ho, Y.-L., 2010. Applying harmonic optical microscopy for spatial alignment of atrial collagen fibers. PLoS ONE 5, e13917.
Cloos, P.A., Fledelius, C., Christgau, S., Christiansen, C., Engsig, M., Delmas, P., Body, J.J., Garnero, P., 2003. Investigation of bone disease using isomerized and racemized fragments of type I collagen. Calcif. Tissue Int. 72, 8–17.
Collins, M.J., Riley, M.S., Child, A.M., Turner-Walker, G., 1995. A basic mathematical simulation of the chemical degradation of ancient collagen. J. Archaeol. Sci. 22, 175–183.
Gu, C., Dinesh, R.K., Katti, K.S., 2013. Photoacoustic FTIR spectroscopic study of undisturbed human cortical bone. Spectrochim. Acta A 102, 25–37.
Gullekson, C., Lucas, L., Hewitt, K., Kreplak, L., 2011. Surface-sensitive Raman spectroscopy of collagen I fibrils. Biophys. J. 100, 1837–1845.
Jiang, X., Ye, M., Jiang, X., Liu, G., Feng, S., Cui, L., Zou, H., 2007. Method development of efficient protein extraction in bone tissue for proteome analysis. J. Proteome Res. 6, 2287–2294.
Lee, Y.-C., Chiang, C.-C., Huang, P.-Y., Chung, C.-Y., Huang, T.D., Wang, C.-C., Chen, C.-I., Chang, R.-S., Liao, C.-H., Reisz, R.R., 2017. Evidence of preserved collagen in an Early Jurassic sauropodomorph dinosaur revealed by synchrotron FTIR microspectroscopy. Nat. Commun. 8, 14220.
Lee-Thorp, J.A., Sealy, J.C., van der Merwe, N.J., 1989. Stable carbon isotope ratio differences between bone collagen and bone apatite, and their relationship to diet. J. Archaeol. Sci. 16, 585–599.
McLaughlin, G., Lednev, I.K., 2011. Potential application of Raman spectroscopy for determining burial duration of skeletal remains. Anal. Bioanal. Chem. 401, 2511–2518.
Mohler, W., Millard, A.C., Campagnola, P.J., 2003. Second harmonic generation imaging of endogenous structural proteins. Methods 29, 97–109.
Monici, M., 2005. Cell and tissue autofluorescence research and diagnostic applications. Biotechnol. Annu. Rev. 11, 227–256.
Morris, M.D., Finney, W.F., 2004. Recent developments in Raman and infrared spectroscopy and imaging of bone tissue. Spectroscopy 18, 155–159.
Morvan-Dubois, G., Le Guellec, D., Garrone, R., Zylberberg, L., Bonnaud, L., 2003. Phylogenetic analysis of vertebrate fibrillar collagen locates the position of zebrafish α3(I) and suggests an evolutionary link between collagen a chains and Hox clusters. J. Mol. Evol. 57, 501–514.
Naik, N., Caves, J., Chaikof, E., Allen, M.G., 2014. Generation of spatially aligned collagen fiber networks through microstransfer molding. Adv. Healthc. Mater. 3, 367–374.
Penel, G., Delfosse, C., Dsescamps, M., Leroy, G., 2005. Composition of bone and apatitic biomaterials as revealed by intravital Raman microspectroscopy. Bone 36, 893–901.
Perkins, D.N., Pappin, D.J., Creasy, D.M., Cottrell, J.S., 1999. Probability-based protein identification by searching sequence databases using mass spectrometry data. Electrophoresis 20, 3551–3567.
Schindelin, J., Arganda-Carreras, I., Frise, E., Kaynig, V., Longair, M., Pietsh, T., Preibisch, S., Rueden, C., Saalfeld, S., Schmid, B., Tinevez, J.-Y., White, Dj, Hartenstein, V., Eliceiri, K., Tomancak, P., Fijí, Cardona A., 2012. An open-source platform for biological-image analysis. Nat. Methods 9, 676–682.
Schrof, S., Varga, P., Galvis, L., Raum, K., Masic, A., 2014. 3D mapping of the collagen fibril orientation in human osteonal lamellae. J. Struct. Biol. 187, 266–275.
Scott, D., Garner, T.P., Long, J., Strachan, J., Mistry, S.C., Bottrill, A.R., Tooth, D.J., Searle, M.S., Oldham, N.J., Layfield, R., 2016. Mass spectrometry insights into a tandem ubiquitin-binding domain hybrid engineered for the selective recognition of unanchored polyubiquitin. Proteomics 16, 1961–1969.
Searle, B.C., 2010. Scaffold: a bioinformatic tool for validating MS/MS-based proteomic studies. Proteomics 10, 1265–1269.
Strupler, M., Pena, A.-M., Hernest, M., Tharaux, P.-L., Martin, J.-L., Beaurepaire, E., Schanne-Klein, M.-C., 2007. Second harmonic imaging and scoring of collagen in fibrotic tissues. Opt. Express 15, 4054–4065.
Surmik, D., Boczarowski, A., Balin, K., Dulski, M., Szade, J., Kremer, B., Pawlicki, R., 2016. Spectroscopic studies on organic matter from Triassic reptile bones, Upper Silesia, Poland. PLoS ONE 11, e0151143.
Thompson, T.J.U., Gauthier, M., Islam, M., 2009. The application of a new method of Fourier transform infrared spectroscopy to the analysis of burned bone. J. Archaeol. Sci. 36, 910–914.
Thompson, T.J.U., Islam, M., Bonniere, M., 2013. A new statistical approach for determining the crystallinity of heat-altered bone mineral from FTIR spectra. J. Archaeol. Sci. 40, 416–422.
Zipfel, W.R., Williams, R.M., Christie, R., Nikitin, A.Y., Hyman, B.T., Webb, W.W., 2003. Live tissue intrinsic emission microscopy using multiphoton-excited native fluorescence and second harmonic generation. PNAS 100, 7075–7080.